A temperature-controlled photoelectrochemical cell for quantitative product analysis

Elizabeth R. Corson, Erin B. Creel, Youngsang Kim, Jeffrey J. Urban, Robert Kostecki, and Bryan D. McCloskey

Citation: Review of Scientific Instruments **89**, 055112 (2018); doi: 10.1063/1.5024802
View online: https://doi.org/10.1063/1.5024802
View Table of Contents: http://aip.scitation.org/toc/rsi/89/5
Published by the American Institute of Physics

A temperature-controlled photoelectrochemical cell for quantitative product analysis

Elizabeth R. Corson,[1,2] Erin B. Creel,[1,3,4] Youngsang Kim,[1] Jeffrey J. Urban,[1,3] Robert Kostecki,[1,5] and Bryan D. McCloskey[1,2,5]
[1]*Joint Center for Artificial Photosynthesis, Lawrence Berkeley National Laboratory, Berkeley, California 94720, USA*
[2]*Department of Chemical and Biomolecular Engineering, University of California, Berkeley, California 94720, USA*
[3]*The Molecular Foundry, Lawrence Berkeley National Laboratory, Berkeley, California 94720, USA*
[4]*Department of Chemistry, University of California, Berkeley, California 94720, USA*
[5]*Energy Storage and Distributed Resources Division, Lawrence Berkeley National Laboratory, Berkeley, California 94720, USA*

(Received 4 February 2018; accepted 30 April 2018; published online 18 May 2018)

In this study, we describe the design and operation of a temperature-controlled photoelectrochemical cell for analysis of gaseous and liquid products formed at an illuminated working electrode. This cell is specifically designed to quantitatively analyze photoelectrochemical processes that yield multiple gas and liquid products at low current densities and exhibit limiting reactant concentrations that prevent these processes from being studied in traditional single chamber electrolytic cells. The geometry of the cell presented in this paper enables front-illumination of the photoelectrode and maximizes the electrode surface area to electrolyte volume ratio to increase liquid product concentration and hence enhances *ex situ* spectroscopic sensitivity toward them. Gas is bubbled through the electrolyte in the working electrode chamber during operation to maintain a saturated reactant concentration and to continuously mix the electrolyte. Gaseous products are detected by an in-line gas chromatograph, and liquid products are analyzed *ex situ* by nuclear magnetic resonance. Cell performance was validated by examining carbon dioxide reduction on a silver foil electrode, showing comparable results both to those reported in the literature and identical experiments performed in a standard parallel-electrode electrochemical cell. To demonstrate a photoelectrochemical application of the cell, CO_2 reduction experiments were carried out on a plasmonic nanostructured silver photocathode and showed different product distributions under dark and illuminated conditions. *Published by AIP Publishing.*
https://doi.org/10.1063/1.5024802

I. INTRODUCTION

Photocatalytic reactions have been widely studied for both semiconducting and plasmonic systems as a means of overcoming high activation barriers and storing solar energy.[1,2] The less-explored field of photoelectrocatalysis (PEC) uses light to excite carriers and enhance the applied electric field to drive the excited carriers to the catalytically active surface. Reaction pathways can be selective to the light intensity, light wavelength, electrochemical potential, or a combination of these factors, all of which can be tuned independently in PEC. Investigating photoelectrochemical reactions requires a vessel that contains electrolyte and permits illumination of the photoelectrode that is immersed in the electrolyte. While a simple single chamber electrolytic cell with a transparent window may be appropriate for the study of well-characterized reactions with a single product, a new photoelectrochemical cell design is needed for more complicated reactions where quantification of multiple gaseous and/or liquid products is required, as in the case of carbon dioxide (CO_2) reduction.

PEC CO_2 reduction can be used for the storage of solar energy by converting CO_2 into renewable fuels such as methane (CH_4) or ethanol (C_2H_4OH). Electrochemical CO_2 reduction suffers from high overpotentials and low selectivity, producing a mixture of gaseous and liquid products.[3,4] Plasmonic hot-carriers and the strong local electric fields produced by plasmon excitation may open new mechanistic pathways for electrochemical reactions.[1,5–7] A PEC cell that allows one to measure how light changes the product distribution is critical to understanding the mechanism of plasmon-enhanced photoelectrochemistry.

To accurately measure these products, the photoelectrochemical cell must be leak-tight, have a small electrolyte volume while maximizing the electrode surface area, maintain CO_2 saturation of the electrolyte, and have a membrane separating the anode and cathode to prevent product transfer between chambers. In addition, the cell must be able to operate isothermally under dark and illuminated conditions, have parallel electrodes to ensure even current distribution, and be constructed from electrochemically stable materials that resist contamination. While we will test the PEC cell presented here for CO_2 reduction, these design considerations apply to any PEC system with multiple products, low current densities, and limiting reactant concentration. Examples include nitrogen reduction

to ammonia and methane oxidation to methanol, ethane, or ethylene.

Our unique PEC cell satisfies these design criteria while simultaneously achieving front-illumination of the photoelectrode. Front illumination of the electrode's active surface is desired over back-illumination, in which the electrode is illuminated through the inactive but ideally transparent back side of the electrode, to remove the need for electrode optical transparency and to maximize the light intensity on the active surface of the electrode. To validate the cell and demonstrate its effectiveness, we present three sets of CO_2 reduction experiments and their corresponding product analyses. First, we compare the product distribution during the reduction of CO_2 on a silver (Ag) foil electrode in the photoelectrochemical cell to the same reaction performed in a common CO_2 reduction electrochemical cell, showing no significant difference in the results. Second, to demonstrate the temperature control of the cell, we reduced CO_2 on Ag foil at four different temperatures ranging from 8 to 45 °C. Finally, we performed PEC CO_2 reduction on a nanostructured Ag electrode and compared the product distribution under light and dark conditions. We show that irradiation of the plasmonic Ag electrode results in the selective promotion of CO_2 reduction to carbon monoxide (CO) over the reduction of water to hydrogen (H_2). The PEC cell and methods presented here provide precise and accurate measurements of multiple gaseous and liquid products while illuminating the active surface of one of the electrodes.

II. PHOTOELECTROCHEMICAL CELL DESIGN

PEC CO_2 reduction is challenging to study due to the low solubility of CO_2 in water and generally low current density which yields a mixture of gaseous and liquid products at low concentrations.[8] Researchers studying electrochemical CO_2 reduction have addressed these issues with CO_2-flow cells that maximize the electrode surface area to electrolyte volume ratio, generally by minimizing the cell volume.[9,10] As a result of the low electrolyte and cell mass in such configurations, these cells are especially susceptible to heating under illumination, making temperature control requisite when studying photoelectrochemical processes. While these cell configurations are effective for dark electrochemistry, no comparable cell exists that allows for front-illumination of the working electrode while still providing all the useful characteristics of the small volume, parallel-electrode cell configurations.[9,10] In particular, the desired design features of a PEC cell include separation of the working and counter chambers for liquid and gaseous product segregation, *in situ* gaseous product sampling for analysis, maximizing the electrode surface area to electrolyte volume ratio to increase liquid product concentration, establishing isothermal conditions during illumination, preventing contamination, maintaining a high concentration of CO_2 in the electrolyte, and ensuring that the working electrode chamber is well-mixed.

Our front-illumination photoelectrochemical cell (PEC cell) was designed based on the dark compression cells reported in the literature.[9,10] These dark compression cells meet several, but not all, of the design criteria for a PEC cell, failing to allow for electrode illumination and temperature control. We modified the aligned parallel plate design to allow front-illumination through a quartz window by offsetting the parallel working and counter electrodes as seen in Fig. 1. The PEC cell is leak-tight and incorporates a membrane to separate the working and counter chambers. CO_2 flows continuously through a glass frit at the bottom of the cell to maintain CO_2-saturation of the electrolyte and to carry the evolved gaseous products to a gas chromatograph (GC) for analysis. The PEC cell is milled from polyether ether ketone (PEEK), a chemically inert hard polymer, and has a 0.43 cm^2/ml surface area to volume ratio (S/V) that allows for high sensitivity in *ex situ* liquid product analysis. For comparison, the cell used by Kuhl *et al.*[9] had a S/V of 0.56 cm^2/ml, and Lobaccaro *et al.*[10] reported a S/V of 0.67 cm^2/ml. Both the working and counter electrodes of our PEC cell have a surface area of 1 cm^2. The cell is sealed around five O-rings and compressed by tightening four screws with wing nuts. A complete list of cell parts is provided in Tables S8 and S9 of the supplementary material.

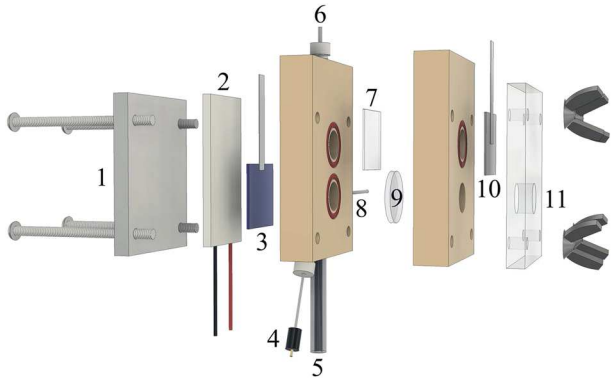

FIG. 1. Schematic of the photoelectrochemical (PEC) cell. The copper and aluminum heat sink (not shown) is secured against the aluminum back plate (1) that transfers heat from the Peltier element (2). The working photoelectrode (3) is in close proximity to the reference electrode (4) and thermistor (8) and is separated from the counter electrode (10) by a membrane (7). Gas enters through the glass frit at the bottom (5) and flows through tubing at the top (6) to the GC for product analysis. A hole in the front plate (11) allows light to shine through the quartz window (9) onto the photoelectrode (3). The total volume of the electrolyte used in the working electrode chamber is 2.3 ml, and the electrode surface areas are 1 cm^2 (1.1 cm diameter).

The reference electrode and thermistor are located in close proximity to the working electrode without blocking the light, as shown in the wireframe view of the working electrode chamber (Fig. 2). As described in more detail later, the temperature can be monitored continuously and controlled within ±0.1 °C during an electrochemical experiment using an external proportional-integral-derivative (PID) controller coupled to a Peltier element located directly behind the working electrode (part 2 in Fig. 1). It typically takes 10–20 min to reach a steady state temperature. In this study, we demonstrate the cell operating from 8 to 45 °C. However, the true operating range is much larger. When using aqueous electrolytes, the cell temperature is limited primarily by the phase transitions of water.

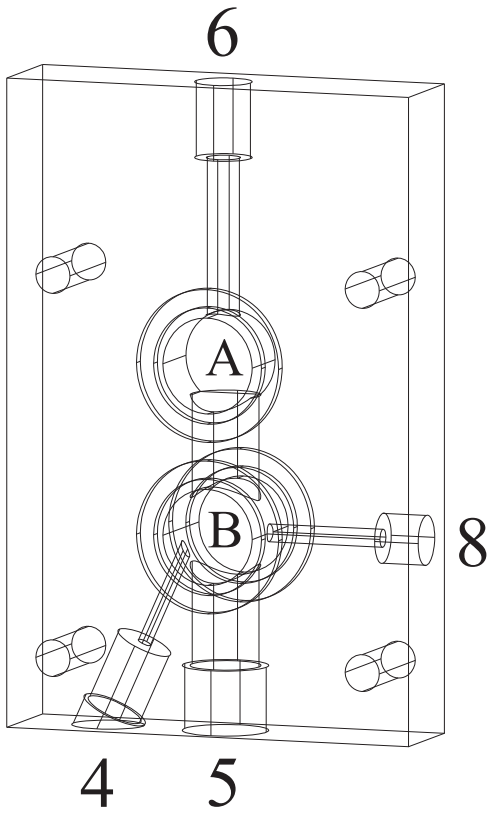

FIG. 2. Wireframe view of the photoelectrode chamber of the PEC cell. As shown in Fig. 1, the gas enters a port at the bottom of the cell (5) and exits through a port at the top of the cell (6). The reference electrode port (4) and the thermistor port (8) enter the bottom chamber (B) near the photoelectrode. The photoelectrode covers the back of the bottom chamber, and the working-chamber electrolyte is connected to the counter-chamber electrolyte through a membrane covering the top chamber (A). A cylindrical bore connects the top and bottom chambers. 2.3 ml of the electrolyte is added to the sealed chamber and entirely fills both the bottom and top chambers.

III. EXPERIMENTAL METHODS

A 0.5M solution of potassium carbonate (K_2CO_3) (Alfa Aesar, 99.997% metals basis) was prepared with 18.2 MΩ deionized water from a Millipore system, which became 1M potassium bicarbonate ($KHCO_3$) when saturated with CO_2 (Praxair, 99.999%). The pH of the saturated electrolyte was 7.57 (Hanna Instruments, pH meter 9124). In the PEC cell, the working chamber was filled with 2.3 ml of the electrolyte and the counter chamber with 0.8 ml. Both chambers of the standard, dark electrochemical cell (EC cell), designed by Lobaccaro *et al.*[10] and used here as a comparison to the PEC cell, were filled with 1.9 ml of the electrolyte (Fig. S6 of the supplementary material).

The Ag foil cathode (thickness 0.1 mm, Alfa Aesar, 99.998% metals basis) was mechanically polished (Norton T401, 2000 grit) before each use. Electrodes with hexagonally arrayed 75 nm Ag nanopyramids were fabricated using nanosphere lithography.[11] See the supplementary material for complete details of electrode fabrication (Fig. S5). The counter electrode was a platinum foil and the reference electrode was a leak-free Ag/AgCl electrode (Innovative Instruments, LF-1, 3.4M KCl). The working and counter chambers were separated by an anion-exchange membrane (AGC Engineering, Selemion AMV).

The cell was sonicated in 20 v/v % nitric acid and deionized water after fabrication and sonicated in deionized water before each use. The chambers of the cell were rinsed with 0.05M K_2CO_3 before adding new electrolyte between consecutive electrolysis measurements on the same cathode. The assembled cell was connected to a gas manifold with leak-tight fittings (IDEX, P-210). A mass flow controller (Alicat, MC-10SCCM-D) set the gas flow rate into the cell. A mass flow meter (Alicat, M-50SCCM-D) placed in line before the gas entered the GC gas-switching valve verified the flow of the controller and was used as a check to ensure the system was leak-free. A CO_2 flow rate of 5.0 SCCM was used for all experiments reported in this study. The CO_2 is bubbled into the electrolyte through a glass frit (Ace Glass, Porosity E).

A. Temperature control

A planar Peltier element (Ferro Tec, 72008/131/150B) was compressed between the aluminum back plate and the cathode. The back plate was attached to a heat sink with a mounted fan (Deep Cool, GAMMAXX 400). The interfaces between the heat sink, back plate, and Peltier element were coated with thermal paste (Chemtronics, CW7250). A thermistor (Microlab, Model 103) covered with a heat-shrink fluorinated ethylene propylene (FEP) probe cover (Tef-Cap Industries) monitored the temperature of the catholyte through the cell side-port. A PID temperature controller (Accuthermo Technology, ATEC302) was used to maintain the catholyte at a constant temperature set point throughout electrolysis. If temperature control is not needed, the Peltier element and heat sink can be removed. In this case, the back plate can be fabricated from a variety of materials including aluminum and polycarbonate.

B. Product analysis

A GC (SRI Instruments, Multiple Gas Analyzer 5) with a 12′ HayeSep D column, argon carrier gas, and a gas-switching valve with a 1 ml sample loop was used for gaseous product analysis. Products separated by the column flow through a Thermal Conductivity Detector (TCD) that detects H_2 followed by a methanizer that converts CO and CO_2 to CH_4 and a Flame Ionization Detector (FID) that detects CH_4, ethylene (C_2H_4), and ethane (C_2H_6) (Fig. S2 of the supplementary material). The GC was calibrated with a set of three calibration gases containing a known mixture of H_2, CO, CH_4, C_2H_4, and C_2H_6 in a balance of CO_2 (Airgas) at concentrations between 100 and 8000 ppm (Table S1 of the supplementary material). A linear calibration curve for each product was calculated from points representing the average of runs repeated multiple times across several days, with the intercept set at zero and R^2 values of 99.89%–99.99% (Table S2 and Fig. S1 of the supplementary material).

Proton nuclear magnetic resonance (^{1}H NMR) spectroscopy (500 MHz Bruker Avance III) was performed for liquid product analysis. 400 μl of an electrolyte sample collected at the end of an experiment was combined with 50 μl of deuterium oxide (D_2O) (Sigma Aldrich, 151882) as the

internal solvent lock and 50 μl of an internal standard comprised of 1 mM phenol in H_2O. A proton water suppression method with a 60 s acquisition time was averaged 16 times. Formate was quantified by comparing the integrated area of the product peak to that of phenol (Table S3 and Figs. S3 and S4 of the supplementary material).[9]

C. Electrochemical measurements

Electrochemical measurements were controlled with a Bio-Logic SP-300 potentiostat. Impedance spectroscopy was used before each experiment to determine the uncompensated electrolyte resistance (R_u). See the supplementary material for detailed IR compensation calculations. The potentiostat compensated for 85% of R_u during electrolysis, where the set potential was applied for 16 min with a GC injection occurring after 15 min. Reported potentials have been converted to a reversible hydrogen electrode (RHE) scale and adjusted for the final 15% of R_u. Each electrochemical experiment was repeated at least three times; reported results are the average of all runs with error bars showing one standard deviation.

D. Photoelectrochemical measurements

The Ag photoelectrode was illuminated by a collimated array of three LEDs (Mightex) with a combined power of 3 W/cm^2 at wavelengths of 385, 405, and 470 nm, which were selected due to their proximity to the reported surface plasmon resonance of Ag.[1] Electrolysis with product analysis was performed as described above under continuous illumination. See the supplementary material for the individual light-emitting diode (LED) power (Table S4) and photocurrent measurements (Fig. S7).

IV. RESULTS AND DISCUSSION

A. Dark CO_2 reduction on a Ag foil electrode

Offset parallel electrodes represent the most straightforward geometry for front illumination of the electrode. However, they also introduce the possibility of non-uniform current distributions across the surface of the electrode. In fact, during initial trials, current instabilities were observed during constant voltage measurements below –0.7 V vs. RHE in 0.1M $KHCO_3$. Current gradients can be suppressed by increasing electrolyte conductivity[12] and thus concentration. We observed a substantial reduction of current instabilities by increasing the concentration of the electrolyte to 1M $KHCO_3$. To determine the impact of offset parallel electrodes at this higher electrolyte concentration, the product distribution and current densities on Ag foil at four different potentials at ambient temperature were measured in the PEC cell as well as the EC cell with aligned parallel electrodes fabricated based on a previously reported design by Lobaccaro *et al.* (Fig. S6 of the supplementary material).[10] Faradaic efficiencies for each product are plotted in Fig. 3, with equations for calculating Faradaic efficiencies for gaseous and liquid products provided in the supplementary material. The observed products were CO, H_2, and formate with an average total Faradaic efficiency of 99.9% across both cells (Fig. S10 of the supplementary material). The results in

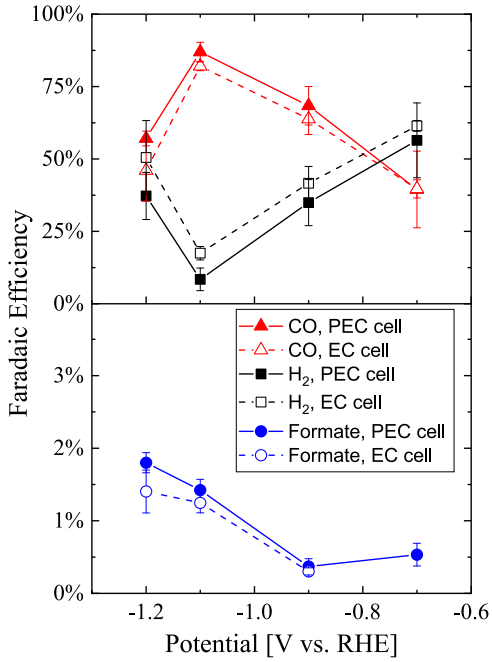

FIG. 3. Faradaic efficiency results after 15 min of electrolysis without illumination at various potentials on Ag foil in 1M $KHCO_3$ with continuous CO_2 flow at 22 °C. The PEC cell results are connected with solid lines (---) and the EC cell results are connected with dashed lines (—) to guide the eye. No formate was detected in the EC cell at –0.7 V vs. RHE.

the PEC cell were remarkably similar to those measured in the EC cell; using a two-sample t-test assuming unequal variances with a significance level $\alpha = 0.05$, there was no statistical difference between the PEC cell and EC cell performance (Table S5 of the supplementary material). In addition, there was no statistical difference between the average current densities at each potential between the PEC cell and the EC cell, which ranged from –0.9 mA/cm^2 to –15 mA/cm^2 (Fig. S8 of the supplementary material). These results indicate that any current distribution due to the offset parallel electrode design of our cell does not impact the product current efficiencies or the overall current density.

Not only are the results in the PEC cell and EC cell nearly identical but they also agree with similar studies reported in the literature.[13] Although minor differences in exact product distributions between prior reports and ours are observed, the trend of CO production going through a maximum at –1.1 V vs. RHE, with H_2 production going through a minimum, is in excellent agreement with prior work.[13] Similarly, the continually increasing trend of formate production with more cathodic potentials also matches those results. Variations in operating conditions may explain the differences between our studies and those previously published; Hatsukade *et al.* used 0.1M $KHCO_3$, flowed CO_2 through tubing at 20 SCCM, and operated for 1 h prior to product analysis.[13]

B. Temperature variation during CO_2 reduction

Like all gases, CO_2 solubility in aqueous electrolytes at moderate temperatures (0-50 °C) decreases with increasing temperature, which in turn can have a profound effect on the

product distribution during electrolysis of CO_2-saturated solutions. Nevertheless, only a few studies have been published on the influence of temperature on CO_2 reduction.[4,14–20] To demonstrate the temperature control capabilities of our PEC cell, we studied constant potential (−1.1 V vs. RHE) electrolysis of CO_2-saturated 1M $KHCO_3$ at a smooth Ag foil electrode at 8, 22, 35, and 45 °C. Figure 4 shows the temperature in the cell over time during a representative 8 °C run; the PID controller brings the cell temperature to the set point without overshooting and stabilizes in 10 min. Over the course of the electrochemical run, the temperature is maintained between 7.9 and 8.1 °C. Fluctuations in the current density are attributed to the high rate of CO_2 bubbling between the working electrode and the reference electrode.

Faradaic efficiencies of CO_2, H_2, and formate at 8, 22, 35, and 45 °C are presented in Fig. 5 and indicate that the selectivity toward CO production is the highest at 8 °C and decreases as the cell temperature is increased with a concomitant increase in H_2 selectivity. Current density, as well as the partial current densities of CO, H_2, and formate, was observed to increase with increasing temperature (Fig. S9 of the supplementary material). In particular, H_2 partial current density, which increased by more than an order of magnitude from 8 °C to 45 °C, was influenced to a much greater extent than CO formation with increasing temperature. These trends are likely a result of diminished CO_2 solubility in the electrolyte, which decreases exponentially with temperature.[10] The lower CO_2 concentration in the electrolyte at higher temperature allows more active sites to reduce water to H_2. However, it is worth noting that the Faradaic efficiency of formate remained constant with varying temperature. Azuma *et al.* similarly saw CO decrease and H_2 increase from 2 °C to room temperature on a Ag electrode in 0.05M $KHCO_3$, although they observed formate decrease with increasing temperature.[14] Hori *et al.* reported increasing H_2 production on Cu in 0.5M $KHCO_3$ with increasing temperature (0–40 °C), and while the total current efficiency of CO_2 reduction products decreased with increasing temperature, CO and C_2H_4 increased, formate remained constant, and CH_4 decreased with increasing temperature.[4] Clearly temperature can affect factors beyond solubility, such as reaction rates, coverage of adsorbed species, and reaction pathways, making it a vital parameter for understanding the fundamental mechanisms of CO_2 reduction.[4,14,21]

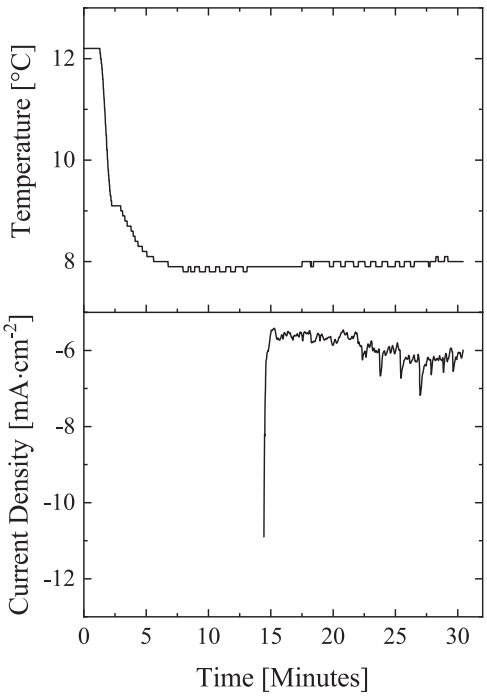

FIG. 4. Electrolysis without illumination of the CO_2-saturated electrolyte at a smooth Ag foil electrode at 8 °C. Cell temperature was maintained using a PID-controlled Peltier element as shown in Fig. 1. In this measurement, the control feedback was started after 1 min of temperature recording with a set point of 8 °C. Electrolysis started at 14 min at −1.1 V vs. RHE on Ag foil in 1M $KHCO_3$ with continuous CO_2 flow in the photoelectrochemical cell.

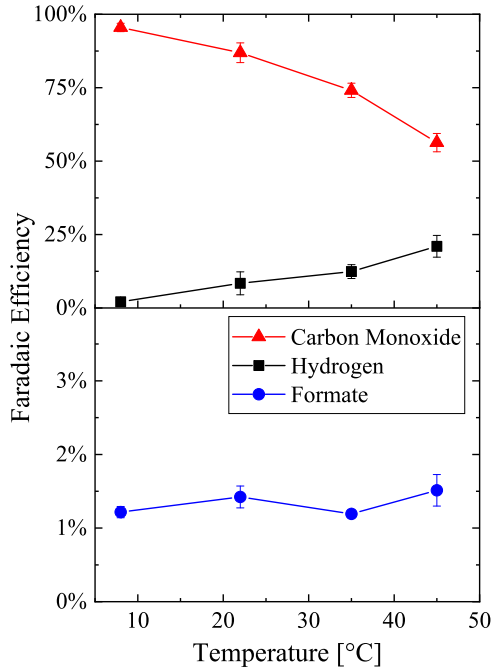

FIG. 5. Faradaic efficiency results after 15 min of electrolysis without illumination at −1.1 V vs. RHE on Ag foil in 1M $KHCO_3$ with continuous CO_2 flow in the photoelectrochemical cell at 8, 22, 35, and 45 °C.

C. Photoelectrochemical CO_2 reduction on a Ag electrode

When studying photoelectrodes, it is critical to separate temperature effects from light effects, particularly because light absorption can cause fast temperature rise in low-volume electrolyte cells. For example, in our small-volume cell, the temperature increased 10 °C in the first 10 min of illumination without temperature control; as seen in Sec. IV B, such a temperature difference can drastically change the product distribution. Without temperature control, it would be impossible to draw meaningful conclusions between results with and without illumination. To demonstrate the isothermal operation of the PEC cell under illumination, we used plasmonic nanostructured Ag electrodes.[8] Figure 6 shows the temperature of the cell over time during a typical experiment with continuous illumination of the photoelectrode. After one minute of temperature recording, the LED array is turned on and the

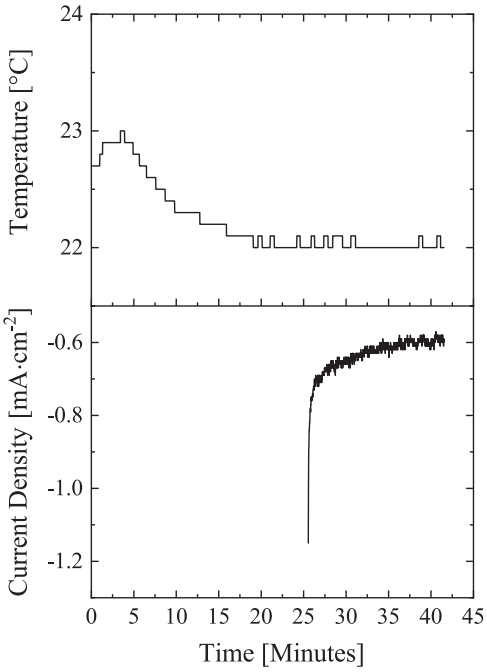

FIG. 6. Temperature control during electrolysis at a front-illuminated photoelectrode using an LED array (385, 405, and 470 nm). Illumination and cell temperature control started after 1 min of temperature recording with a set point of 22 °C. Continuous illumination and temperature control were maintained when electrolysis started at 26 min; –0.8 V vs. RHE on a nanostructured Ag electrode (described in the supplementary material) in 1M $KHCO_3$ with continuous CO_2 flow through the cell.

temperature control is started with a set point of 22 °C. The LED illumination initially causes the temperature to rise by 0.3 °C before the temperature controller cools the cell to the set point temperature within 20 minutes. Once the set point is achieved, the system is held within 0.1 °C of the desired temperature for the duration of the electrochemical experiment. PID tuning was important to ensure that temperature set point overshoot was not observed (Table S7 of the supplementary material).

The product distribution from electrolysis at the nanostructured Ag electrodes in the dark and under continuous illumination at an applied potential of −0.8 V vs. RHE is shown in Fig. 7. Interestingly, under the same applied potential and temperature, the product distribution changes when the surface of the plasmonic electrode is illuminated. CO production increases from 55% to 68% in the light and formate generation increases from 0.3% to 1.0%. This difference in product distribution is statistically significant, as determined by a two-sample t-test assuming unequal variances with $\alpha = 0.05$ (Table S6 of the supplementary material). At this potential, the photocurrent was 0.14 mA/cm^2, which is 10% of the total current density (Fig. S7 of the supplementary material). The 13% increase in CO_2 reduction products over H_2 evolution correlates with the magnitude of the photocurrent at the applied voltage.

As further evidence of effective temperature control, the results in Sec. IV B indicate that if the difference in product distribution between dark and light conditions were due to heating, we would expect to see an increase in H_2 evolution rather than CO. In previous studies, plasmon-enhanced CO

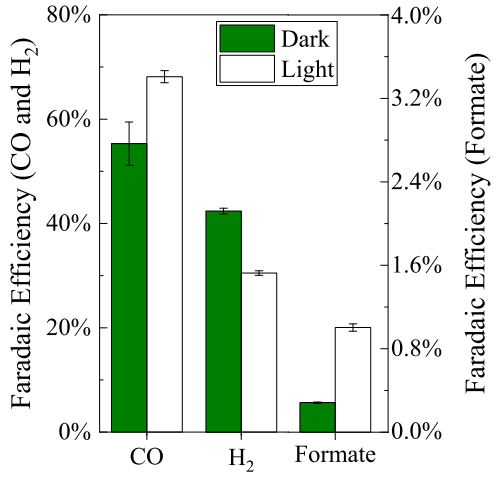

FIG. 7. Faradaic efficiency results after 15 min of electrolysis at −0.8 V vs. RHE on nanostructured Ag electrodes in 1M $KHCO_3$ with continuous CO_2 flow in the photoelectrochemical cell at 22 °C. Dark indicates no illumination and light indicates continuous illumination by the LED array (385, 405, and 470 nm).

production was hypothesized when a large photocurrent was observed on nanostructured Ag electrodes in CO_2-saturated electrolytes, but a negligible photocurrent was observed in Ar-saturated electrolytes.[8,22–24] While some groups have shown photocatalytic CO_2 reduction on plasmonic electrodes,[25–29] this is the first demonstration of a change in the product distribution driven by plasmon-enhanced photoelectrochemical CO_2 reduction. Further investigation using our PEC cell will shed light on the mechanism of plasmonic CO_2 electrochemical reduction, which is not yet known. The selectivity change under illumination highlights the need to understand the role of light in CO_2 reduction at plasmonically active electrodes, which requires the careful measurement of products as this cell allows.

V. CONCLUSIONS

We have designed a photoelectrochemical cell for studying challenging systems which evolve multiple gaseous and/or liquid products and possess low current densities and limiting reactant concentrations. While the cell can be adapted to many reactions, we demonstrate its efficacy for the CO_2 reduction reaction in this manuscript. We show our cell is effective for studying photoelectrochemical CO_2 reduction and the influence of illumination on photoactive electrodes. We have shown that our PEC cell can match the results of a standard electrochemical cell while incorporating the additional features of temperature control and allowing front-illumination of the working electrode. The plasmonic nanostructured Ag electrode was shown to selectively promote CO_2 reduction to CO over H_2 evolution upon illumination. In future work, we will use this cell to fully characterize nanostructured plasmonic electrodes to understand the mechanism of plasmon-enhanced CO_2 reduction.

SUPPLEMENTARY MATERIAL

See supplementary material for further details on GC calibration, liquid product quantification by NMR, electrode

fabrication, the standard electrochemical cell, electrochemical techniques, statistical analysis, and temperature control.

ACKNOWLEDGMENTS

We thank Davis Perez, Matthew Liu, Dr. Fen Qiu, Ezra Clark, Professor Alex Bell, Dr. Yanwei Lum, Aya Buckley, Dr. Gideon Segev, Dr. Jason Cooper, Dr. Chang-Ming Jiang, Dr. Peter Lobaccaro, Jeff Beeman, and David Larson for useful discussions. This material is based upon work performed by the Joint Center for Artificial Photosynthesis, a DOE Energy Innovation Hub, supported through the Office of Science of the U.S. Department of Energy under Award No. DE-SC0004993. This material is based upon work supported by the National Science Foundation under Grant No. CBET-1653430. Work at the Molecular Foundry was supported by the Office of Science, Office of Basic Energy Sciences, of the U.S. Department of Energy under Contract No. DE-AC02-05CH11231. E.R.C. and E.B.C. acknowledge support from the National Science Foundation Graduate Research Fellowship under Grant No. DGE 1106400.

[1] S. Linic, P. Christopher, and D. B. Ingram, Nat. Mater. **10**, 911 (2011).
[2] H. Tong, S. Ouyang, Y. Bi, N. Umezawa, M. Oshikiri, and J. Ye, Adv. Mater. **24**, 229 (2012).
[3] Y. Hori, K. Kikuchi, and S. Suzuki, Chem. Lett. **14**, 1695 (1985).
[4] Y. Hori, K. Kikuchi, A. Murata, and S. Suzuki, Chem. Lett. **15**, 897 (1986).
[5] S. Mukherjee, L. Zhou, A. M. Goodman, N. Large, C. Ayala-Orozco, Y. Zhang, P. Nordlander, and N. J. Halas, J. Am. Chem. Soc. **136**, 64 (2014).
[6] A. O. Govorov, H. Zhang, H. V. Demir, and Y. K. Gun'ko, Nano Today **9**, 85 (2014).
[7] R. Sundararaman, P. Narang, A. S. Jermyn, W. A. Goddard, and H. A. Atwater, Nat. Commun. **5**, 5788 (2014).
[8] Y. Kim, E. B. Creel, E. R. Corson, B. D. Mccloskey, J. J. Urban, and R. Kostecki, "Surface Plasmon-Assisted Photoelectrochemical Reduction of CO_2 and NO_3^- on Nanostructured Silver Electrodes," Adv. Energy Mater. (to be published).
[9] K. P. Kuhl, E. R. Cave, D. N. Abram, and T. F. Jaramillo, Energy Environ. Sci. **5**, 7050 (2012).
[10] P. Lobaccaro, M. R. Singh, E. L. Clark, Y. Kwon, A. T. Bell, and J. W. Ager, Phys. Chem. Chem. Phys. **18**, 26777 (2016).
[11] G. H. Chan, J. Zhao, E. M. Hicks, G. C. Schatz, and R. P. V. Duyne, Nano Lett. **7**, 1947 (2007).
[12] A. C. West, *Electrochemistry and Electrochemical Engineering: An Introduction* (Columbia University, New York, 2013).
[13] T. Hatsukade, K. P. Kuhl, E. R. Cave, D. N. Abram, and T. F. Jaramillo, Phys. Chem. Chem. Phys. **16**, 13814 (2014).
[14] M. Azuma, K. Hashimoto, M. Hiramoto, M. Watanabe, and T. Sakata, J. Electroanal. Chem. Interfacial Electrochem. **260**, 441 (1989).
[15] M. Azuma, K. Hashimoto, and M. Hiramoto, J. Electrochem. Soc. **137**, 1772 (1990).
[16] A. Kudo, S. Nakagawa, A. Tsuneto, and T. Sakata, J. Electrochem. Soc. **140**, 1541 (1993).
[17] T. Mizuno, K. Ohta, A. Sasaki, T. Akai, M. Hirano, and A. Kawabe, Energy Sources **17**, 503 (1995).
[18] A. Gennaro, A. A. Isse, M. Severin, E. Vianello, I. Bhugun, and J. Saveant, J. Chem. Soc., Faraday Trans. **92**, 3963 (1996).
[19] S. Kaneco, K. Iiba, K. Ohta, T. Mizuno, and A. Saji, Electrochim. Acta **44**, 573 (1998).
[20] S. Kaneco, K. Iiba, K. Ohta, T. Mizuno, and A. Saji, J. Electroanal. Chem. **441**, 215 (1998).
[21] R. P. S. Chaplin and A. A. Wragg, J. Appl. Electrochem. **33**, 1107 (2003).
[22] R. Kostecki and J. Augustynski, Chem. Phys. Lett. **194**, 386 (1992).
[23] R. Kostecki and J. Augustynski, J. Appl. Electrochem. **23**, 567 (1993).
[24] R. Kostecki and J. Augustynski, J. Appl. Phys. **77**, 4701 (1995).
[25] W. Hou, W. H. Hung, P. Pavaskar, A. Goeppert, M. Aykol, and S. B. Cronin, ACS Catal. **1**, 929 (2011).
[26] E. Liu, L. Kang, F. Wu, T. Sun, X. Hu, Y. Yang, H. Liu, and J. Fan, Plasmonics **9**, 61 (2013).
[27] C. Wang, O. Ranasingha, S. Natesakhawat, P. R. Ohodnicki, Jr., M. Andio, J. P. Lewis, and C. Matranga, Nanoscale **5**, 6968 (2013).
[28] K. Choi, D. Kim, B. Rungtaweevoranit, C. A. Trickett, J. T. D. Barmanbek, P. Yang, and O. M. Yaghi, J. Am. Chem. Soc. **139**, 356 (2017).
[29] X. Zhang, X. Li, D. Zhang, N. Q. Su, W. Yang, H. O. Everitt, and J. Liu, Nat. Commun. **8**, 14542 (2017).